Robust energy selective tunneling readout of singlet triplet qubits under large magnetic field gradient

Wonjin Jang[1†], Jehyun Kim[1†], Min-Kyun Cho[1], Hwanchul Chung[2], Sanghyeok Park[1], Jaeun Eom[1], Vladimir Umansky[3], Yunchul Chung[2], and Dohun Kim[1]*

[1]*Department of Physics and Astronomy, and Institute of Applied Physics, Seoul National University, Seoul 08826, Korea*

[2] *Department of Physics, Pusan National University, Busan 46241, Korea*

[3]*Braun Center for Submicron Research, Department of Condensed Matter Physics, Weizmann Institute of Science, Rehovot 76100, Israel*

[†]*These authors contributed equally to this work*

**Corresponding author: dohunkim@snu.ac.kr*

Supplementary Information

Supplementary Note 1. Electron temperature and intra-qubit tunnel coupling calibration

Electron temperature, and the tunnel coupling strength of the left double quantum dot are measured using the standard lock-in technique. dV_{rf}/dV_2 is observed by modulating V_2 gate voltage with 337Hz frequency. With proper adjustment of dot-reservoir tunnel rates less than 1 MHz and setting minimal modulation amplitude, the electron temperature T_e ~ 230mK is determined by fitting the heterodyne detected single electron transition line to the equation $\frac{dV_{rf}}{dV_2}(V_1) = A_{offset} - \frac{A\alpha}{k_B T}\frac{\exp(\alpha(V_1 - V_{offset})/k_B T)}{(1+\exp(\alpha(V_1 - V_{offset})/k_B T))^2}$, which is the derivative of the typical Fermi-Dirac distribution (Supplementary Fig. 1a). Here $\alpha = 0.035$ is the lever-arm of the V_1 gate obtained from the Coulomb diamond measurement, k_B is the Boltzmann constant, and A_{offset} and V_{offset} are the dV_{rf}/dV_2 offset and the offset V_1 voltage in the dV_{rf}/dV_2 – V_1 plot, respectively. The intra-qubit tunnel coupling strength t_c was obtained in the similar manner, by sweeping the gate voltage through the inter-dot transition line in the stability diagram for example shown in Fig. 1c of the main text. The broadening is fitted using the same equation described above, with the broadening width $2t_c$ instead of $k_B T$ where the t_c represents the tunnel coupling strength. The resultant $2t_c/h$ is 16 GHz where h is the Plank's constant.

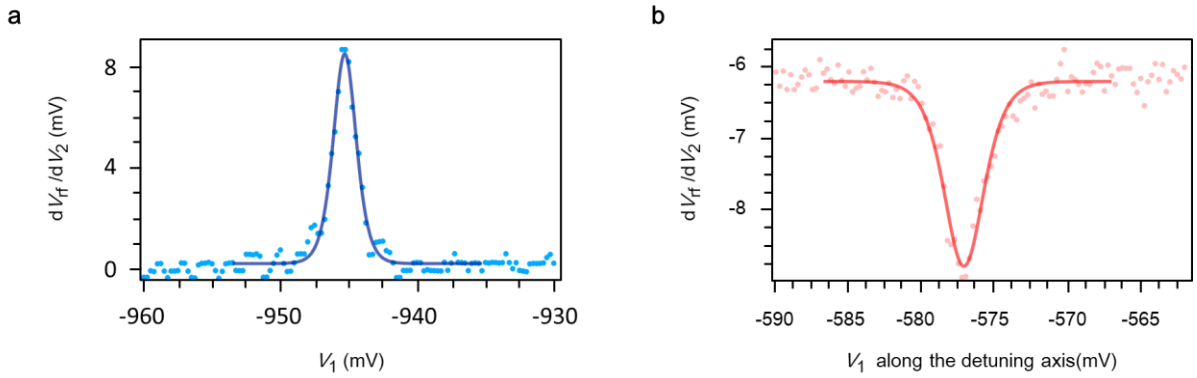

Supplementary Figure 1. System parameter calibration. a. Electron temperature measurement. **b.** tunnel coupling strength measurement using the heterodyne detection scheme. Typical lock-in measurement was performed to obtain the broadening of the single electron transition due to thermal broadening and the intra-qubit tunneling. Electron temperature T_e ~ 230 mK, and tunnel coupling t_c/h ~ 8GHz were obtained from the fitting. When obtaining **b.** both V_1, and V_2 were swept through the inter-dot transition line in Fig. 1c, but only the V_1 gate voltage is shown in the x-axis.

Supplementary Note 2. Correlated double sampling (CDS)

By resampling the demodulated rf-signal with the boxcar integrator, we enable the real-time single-shot event counting without the use of field-programmable gate arrays (FPGA) programming. As shown in Supplementary Fig. 2, the boxcar integrator subtracts the 100 ns-averaged baseline signal from the gate signal which are separated by 5 μs in the time domain to yield a pseudo-time derivative signal of the single-shot trace with 200 kHz sampling rate. CDS converts the falling (rising) edge to the positive (negative) peak and the peaks are detected by the external photon counter (Stanford Research Systems SR400) as shown in Supplementary Fig. 2a. This allows the separate detection of tunneling in / out event in real-time without post-processing which may reduce the experimental overhead in the analysis step. By counting the tunneling out events, we have observed the coherent singlet-triplet qubit (ST_0 qubit) oscillations in the energy selective tunneling (EST) readout point in the main text. For single-shot readout, the boxcar integrator is operated with average number set to 1 (no averaging).

When averaged, however, the CDS technique can also be utilized to observe short-lived T_0 signal for Pauli Spin Blockade (PSB) readout, which enable measurement bandwidth of 33MHz in time averaged manner (see also the inset to Fig. 1c in the main text). By setting the ~ 0.1 μs gate window right after the spin-mixing pulse comes back to the PSB region, and the ~ 0.1 μs baseline gate window before the next pulse start as shown in Supplementary Fig. 2b, the demodulated signal is effectively sampled for short time where the portion of the T_0 signal is sufficiently large to be observed with sufficient periodic average.

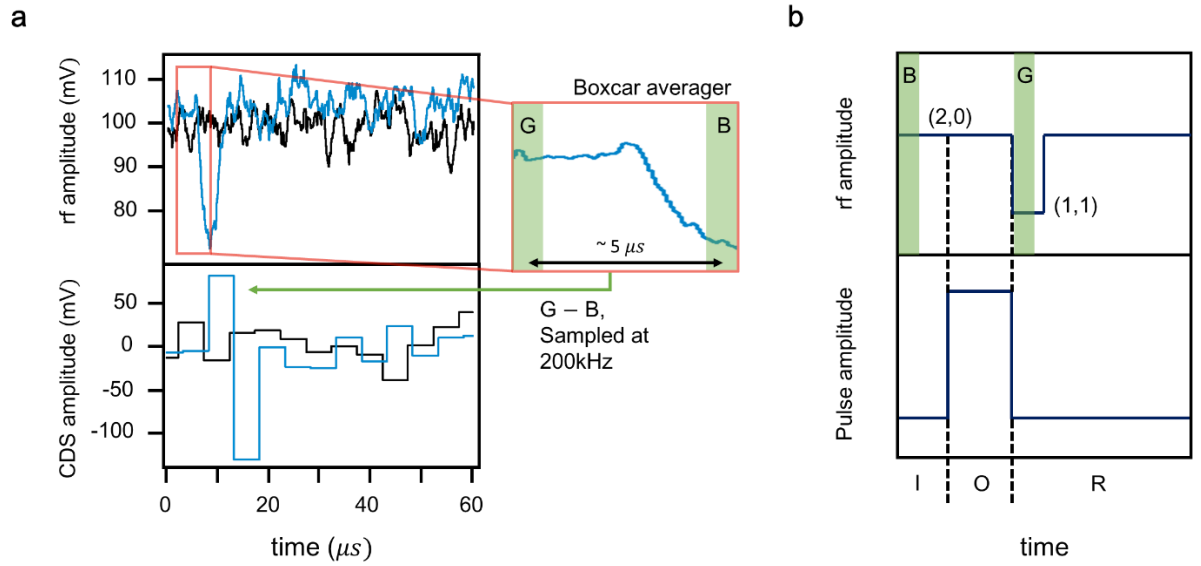

Supplementary Figure 2. Correlated double sampling schematics. a. Correlated double sampling for tunneling out / in event detection. Boxcar integrator resamples the bare demodulated rf signal by subtracting the ~ 100 ns averaged baseline (B) signal from the gate (G) signal every 5 μs . This resampling process converts the falling edge signal of the rf signal to a positive peak with removing dc background and produces pulse signal robust to background drift. **b.** CDS scheme for short T_0 signal detection in PSB readout. Pulse mixes the S and T_0 states in the operation (O) sequence, and when returning to the readout (R) step, the T_0 quickly relaxes to (2,0) charge state under large magnetic field difference. The boxcar integrator in this case is operated in averaging mode where sampled signal G of the rf-signal for short period time after the pulse sequence are subtracted by the B signal and averaged about 5000 times to increase signal to noise ratio.

Supplementary Note 3. Right qubit measurement fidelity

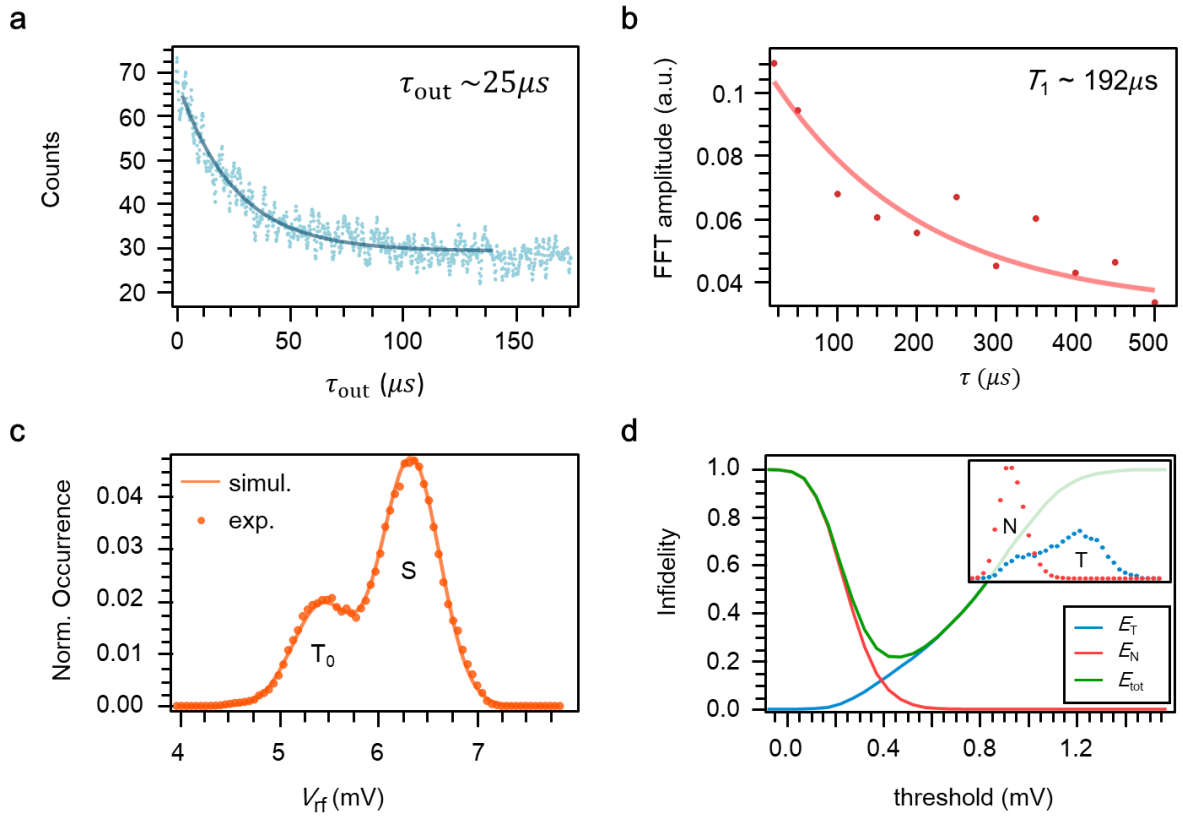

Supplementary Figure 3. Right qubit readout fidelity analysis. a. Tunneling out rate of the right qubit Q_R at the EST readout point. Tunneling out events were recorded as a function of the tunneling time, and the exponential fit to the curve yields $\tau_{out} \sim 25\mu s$. **b.** Relaxation time measurement near EST readout point. The decay of the coherent oscillation is observed along the waiting time τ near the EST readout point. $T_1 \sim 192\ \mu s$ is extracted from the fit. **c.** Experimental, and simulated rf single-shot traces of the Q_R with the π-pulse applied. **d.** Tunneling detection infidelity calculated from the CDS peak amplitude histogram shown in the inset. Minimum total error ($E_T + E_N$) of 28.2% corresponding to $E_T \sim 19\%$, and $E_N \sim 9.2\%$ are estimated at the optimal threshold.

Supplementary Note 4. Magnetic field simulation

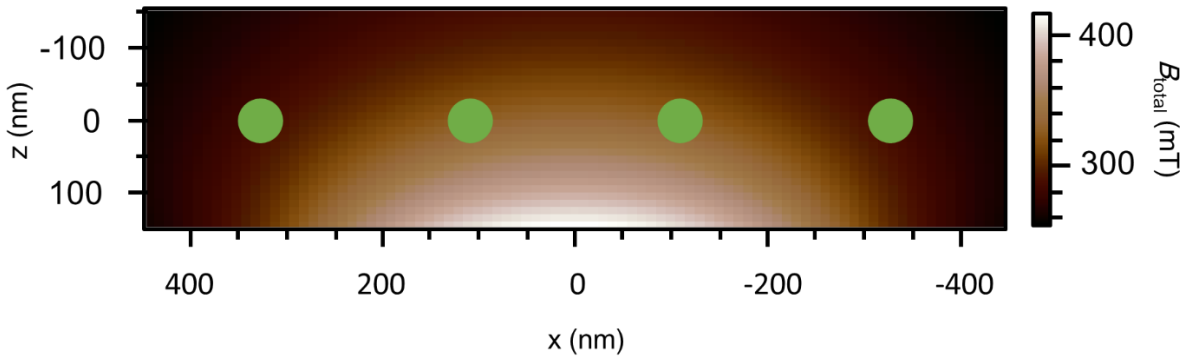

Supplementary Figure 4. Simulation of the magnetic field around the QDs. The total magnetic field strength around the quantum dots in our device (see Supplementary Fig. 8) is simulated using the boundary integral method with RADIA[1,2] package. Green dots indicate the quantum dot positions. The fast $\Delta B_{//}$ oscillations shown in Fig. 3 in the main text is up to 500MHz corresponding to $\Delta B_{//}$ of 100 mT, and we ascribe this higher-than-expected-$\Delta B_{//}$ to the displacement of the electrons from the expected positions by the confining potential in the few electron regime.

Supplementary Note 5. Measurement fidelity analysis

We have taken the thermal tunneling events into consideration for the fidelity analysis and describe the analysis protocol in detail here. We first define two parameters α_1, and β where α_1 corresponds to the probability for the ground (S) state to tunnel out to the reservoir within a measurement window, and β corresponds to the false initialization probability following the Pla. *et al.*[3]. Regarding the false initialization we assume the following for three triplet states – T_0, T_+, and T_-.

1) Probabilities for the electron to falsely initialize to different triplet states are all equal to $\beta/3$.

2) The relaxation time is equal for all T_0, T_+, and T_- state.

3) $T_+(1,1)$, and $T_-(1,1)$ states do not evolve to other states during the Larmor oscillation phase.

It should be noted that while the false initialization to T_0 state contribute to the visibility loss while the false initialization to T_+ or T_- states would result in overall shift of the Larmor oscillation because the T_+ or T_- will not undergo coherent mixing process during the evolution time. We introduce an additional parameter, α_2 to account for the double-tunneling probability of the ground state within a single measurement window. For example, in the case that a T_0 state first tunnels out to the reservoir and initialize to the S state in a measurement phase, there still exist non-zero probability for the S state to tunnel out within the measurement window, and α_2 represents the corresponding probability. It is thus natural to define the total double tunneling probability as $P_2 = (\beta + (1-\beta)\alpha_2)$ which covers the double-tunneling probability of the false initialized triplet states and the reinitialized S state after a single tunneling event.

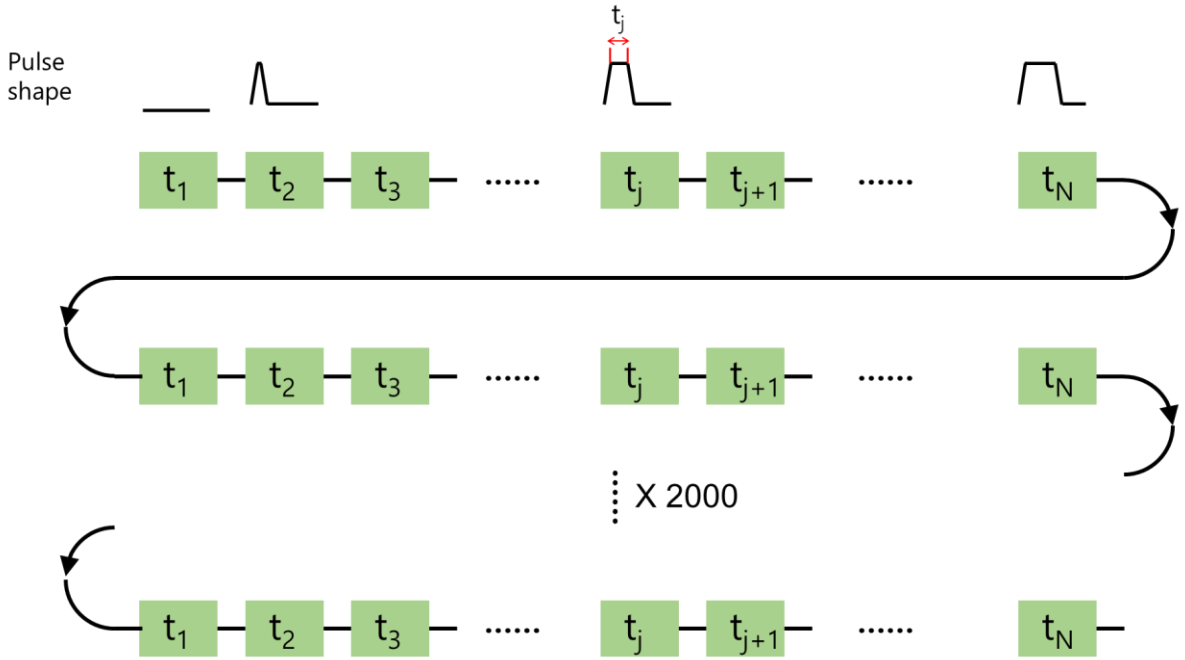

Supplementary Figure 5. Pulse sequence for Larmor oscillation measurement. The Larmor oscillations of Q_L and Q_R are measured by first sweeping the pulse parameter, the free evolution time t_j, and repeating the measurement over 2000 times to average traces. N different pulses corresponding to N different evolution time are all recorded in the arbitrary waveform generator (AWG) before measurements to enable the rapid hardware triggered sweep of the pulse parameter.

In the Larmor experiment in Supplementary Fig. 3a, 3d of the main text, we obtain the oscillation by averaging single-shot traces using the pulse sequence shown in Supplementary Fig. 5. As we regard the spin state is at the excited (T_0) state if there is at least one tunneling event within a measurement window, we first define the $P(t_j, \Delta B_{//})$ as the probability for at least one tunneling to occur within a single measurement window at the evolution time t_j ($1 \le j \le N$, j is integer) under the magnetic field difference $\Delta B_{//}$. It should be noted that $P(t_j, \Delta B_{//})$ must be derived recursively since the tunneling event at the j^{th} shot affects the tunneling probability of the $(j+1)^{th}$ shot. The relation between the $P(t_{j+1}, \Delta B_{//})$, and $P(t_j, \Delta B_{//})$ is as follows.

$$\begin{aligned} P(t_{j+1}, \Delta B_{//}) = P(t_j, \Delta B_{//})[(1-\beta)\{f_{j+1}r + (1-f_{j+1})\alpha_1 + f_{j+1}(1-r)\alpha_1\} + \\ \frac{\beta}{3}\{f_{j+1}\alpha_1 + (1-f_{j+1})r + (1-f_{j+1})(1-r)\alpha_1\} + \\ \frac{2\beta}{3}\{r + (1-r)\alpha_1\}] + \\ (1-P(t_j, \Delta B_{//}))(f_{j+1}r + (1-f_{j+1})\alpha_1 + f_{j+1}(1-r)\alpha_1) \end{aligned} \quad \text{- (1)}$$

Here $f_{j+1} = f(t_{j+1}, \Delta B_{//}) = \sin^2(\pi \Delta B_{//} t_{j+1})$ is the ideal T_0 probability at the evolution time t_{j+1} under the magnetic field difference $\Delta B_{//}$ when the initial state is the singlet state, and (1- r) is the relaxation probability of the T_0 state within the measurement window which is given by $r = \frac{\int_0^M \exp(-t/T_1)\exp(-t/\tau_{out})dt}{\int_0^\infty \exp(-t/\tau_{out})dt}$ where M is the length of the measurement window, T_1 is the spin-relaxation time, and τ_{out} is the tunneling-out time.

However, recursively obtained $P(t, \Delta B_{//})$ cannot yet fully account for the experimentally obtained Larmor curve. We additionally define tunneling detection fidelity T_T (T_N) which is the fidelity to correctly tell there is a (no) tunneling event when there is a (no) peak in the signal. Here T_T and T_N are determined by the signal to noise ratio (SNR) of the measurement setup, and the detailed description on how to obtain the tunneling detection fidelities is given below. With $P(t, \Delta B_{//})$, T_T, and T_N, the experimental Larmor curve can be fully modeled. $A(t, \Delta B_{//})$, the average number of the tunneling events detected by the photon counter, has the following relation with the $P(t, \Delta B_{//})$.

$$A(t, \Delta B_{//}) = P(t, \Delta B_{//})(1 + P_2)T_T + (1 - P(t, \Delta B_{//}))(1 - T_N) \quad \text{- (2)}$$

Assuming that $\Delta B_{//}$ suffers from the Gaussian noise, we perform the Gaussian weighted sum of $A(t, \Delta B_{//})$ curves as below within the 5-sigma range.

$$\bar{A}(t, \Delta B_{//}) = \sum_{b=\Delta B_{//}-5\sigma}^{\Delta B_{//}+5\sigma} A(t, b)\, G(b, \Delta B_{//}, \sigma)\Delta b \quad \text{- (3)}$$

Here $G(x, \mu, \sigma)$ is the Gaussian distribution centered at μ with the standard deviation σ.

By setting α_1, α_2, β, σ, and $\Delta B_{//}$ as the fitting parameters we perform the least squares fitting of the $\bar{A}(t, \Delta B_{//})$ to the experimental Larmor curve. Below we describe the protocol for obtaining the tunneling detection infidelities.

Typical measurement fidelities are acquired by obtaining the histograms of the time-resolved signals of qubit ground and excited states, and finding the adequate threshold which yields the highest visibility[4–6]. The obtained measurement fidelities not only suffer from the imperfect tunneling detection, but also from the spin-relaxation or thermal tunneling events, implying that the T_T, and T_N cannot be solely obtained experimentally. We first numerically simulate[6] the traces with the experimental parameters including the offset rf-voltage, amplitude of the tunneling peaks, tunneling in/out time, spin-relaxation (T_1) time, and sampling rate (Parameters are denoted in the Supplementary Table 1.). The thermal tunneling events are added to the signals in according to the thermal tunneling parameters α_1, α_2 and β, which then undergo through the numerical noise and low pass filter to yield a realistic signal. Then the amplitude of the noise filter is varied to match the experimentally obtained histogram of the rf-signal as in Fig. 2d, and the optimal noise amplitude is chosen. With the noise amplitude,

we numerically generate the 'ideal' signals of triplets and singlets without the thermal tunneling events, or spin-relaxation to solely evaluate the tunneling detection fidelity of the electrical measurement setup. As we have utilized the CDS technique as described in Supplementary Note 2, corresponding boxcar filter is applied to the numerical signals, and the histograms of the boxcar-filtered signals are acquired to perform a typical integration for tunneling detection fidelity calculation[4–6]. We have plotted the tunneling detection infidelity E_{T} (E_{N}) where $E_{\mathrm{T}} = 1 - T_{\mathrm{T}}$ ($E_{\mathrm{N}} = 1 - T_{\mathrm{N}}$) in the Fig.2e and Supplementary Fig. 3d. The tunneling detection fidelities $T_{\mathrm{T}}(V_{\mathrm{op}})$, and $T_{\mathrm{N}}(V_{\mathrm{op}})$ at the optimal threshold which yields the lowest $E_{\mathrm{tot}}(V_{\mathrm{op}}) = E_{\mathrm{T}}(V_{\mathrm{op}}) + E_{\mathrm{N}}(V_{\mathrm{op}})$ are utilized for the Larmor curve fitting described above.

To sum up, the whole process is done as follows.

1) Put the initial guesses of parameters to perform Larmor curve fitting, and obtain the α_1 , α_2 ,and β
2) Use the obtained thermal tunneling parameters for rf-histogram fitting to acquire the optimal noise amplitude.
3) Generate ideal traces of the T_0, and S states with the noise amplitude from 2), and calculate T_{T} , and T_{N}
4) Use T_{T} , and T_{N} for Larmor curve fitting, and obtain α_1 , α_2 , and β .
5) Iteratively obtain the optimal T_{T} , T_{N} , α_1 , α_2 , and β .

We now turn to discuss the total measurement fidelity. If there exist thermal tunneling events irrelevant with the spin dynamics, it is difficult to tell whether the tunneling peak occurs due to the thermal effect or not upon acquiring a single-shot trace. Thereby the total measurement fidelity should now be obtained by taking α_1 , α_2 , and β into account. Let us define $F_{\mathrm{T_0}}$ (F_{S}) as the T_0 (S) measurement fidelity, and $R_{\mathrm{T_0}}(R_{\mathrm{S}}) = 1 - F_{\mathrm{T_0}}(F_{\mathrm{S}})$ as the measurement infidelity. We first evaluate R_{S} by categorizing the cases which can detract the S measurement fidelity.

X_1: No tunneling occurs ($1-\alpha_1$), photon counter 'beeps' due to electrical noise (E_{N})

X_2: A single tunneling occurs (α_1), photon counter detects the tunneling ($1-E_{\mathrm{T}}$)

X_3: A single tunneling occurs (α_1), the tunneling is not detected (E_{T}) but the photon counter 'beeps' due to electrical noise (E_{N})

X_4: Double tunneling occurs ($\alpha_1 P_2$), first tunneling is not detected (E_{T}), and the second tunneling is detected ($1-E_{\mathrm{T}}$)

X_5: Double tunneling occurs ($\alpha_1 P_2$), both tunneling events are not detected ($E_{\mathrm{T}}^{\,2}$), but photon counter 'beeps' due to electrical noise (E_{N})

As X_1 ~ X_5 are independent, mutually exclusive, $R_S = P(X_1) + P(X_2) + P(X_3) + P(X_4) + P(X_5)$ holds. i.e.

$$R_S = (1-\alpha_1)E_N + \alpha_1(1-E_T) + \alpha_1 E_T E_N + \alpha_1 P_2 E_T(1-E_T) + \alpha_1 P_2 {E_T}^2 E_N \quad \text{- (4)}$$

Cases for the T_0 measurement infidelity can be similarly categorized with the relaxation process considered, as follows.

Y: T_0 relaxes within the measurement time $(1-r)$, photon counter detects no tunneling $(1-R_S)$

Z_1: T_0 does not relax within the measurement time (r), the tunneling is not detected (E_T), no additional tunneling occurs $(1-P_2)$, counter detects no signal $(1-E_N)$

Z_2: T_0 does not relax within the measurement time (r), double-tunneling occurs (P_2), both tunneling events are not detected (${E_T}^2$)

Y, Z_1, Z_2 are all independent, and mutually exclusive leading to $R_{T_0} = P(Y) + P(Z_1) + P(Z_2)$. i.e.

$$R_{T_0} = (1-r)(1-R_S) + rE_T(1-P_2)(1-E_N) + r{E_T}^2 P_2 \quad \text{- (5)}$$

Finally, the total measurement fidelity $F_{meas} = 1 - \dfrac{(R_S + R_{T_0})}{2}$ with the spin-relaxation, thermal tunneling events, and the tunneling detection infidelity of the setup is calculated as $90 \pm 1.3\%$ (80.3 ± 1 %) corresponding to visibility($F_S + F_{T_0} - 1$) of 80 ± 2.6 % (60.6 ± 2 %) for Q_L (Q_R). Also, from the Larmor curve fitting we obtain the $\Delta B_{//}$ fluctuation of σ ~15.71 MHz (15.73 MHz) corresponding to T_2^* ~ 14.33 ns (14.31 ns) for Q_L (Q_R). We assume that ~ 3% disagreement of the Q_R visibility is due to the uncertainty in measured relaxation time.

Input	**Q_L**	**Q_R**
τ_{out} (μs) –:Tunneling-out time of the triplet states	16	25.5
τ_{in} (μs) : Tunneling-in time of the singlet state	117	130.5
T_1 (μs) : Relaxation time of the triplet states	337	192
Meas. Time (μs)	150	200
Sampling rate (MHz)	14	14
CDS freq. (kHz)	200	50
CDS gate width (μs)	0.1	4
Output		
α_1 : False tunneling-out probability of the singlet state	0.081	0.092
α_2 : Double tunneling-out probability	0.08	0.089
β : False initialization probability	0.12	0.069
σ (MHz) : Std. deviation of the $\Delta B_{//}$ distribution	15.71	15.73
E_T : Tunneling detection infidelity	0.05	0.19
E_N : No-tunneling detection infidelity	0.055	0.092
R_{T_0} : T_0 measurement infidelity	0.077	0.232
R_S : S measurement infidelity	0.128	0.162
F_{meas} : Total measurement fidelity	90±1.3%	80.3±1 %

Supplementary Table 1. Input and output parameters of the analysis

Supplementary Note 6. Expected fidelity with direct peak detection

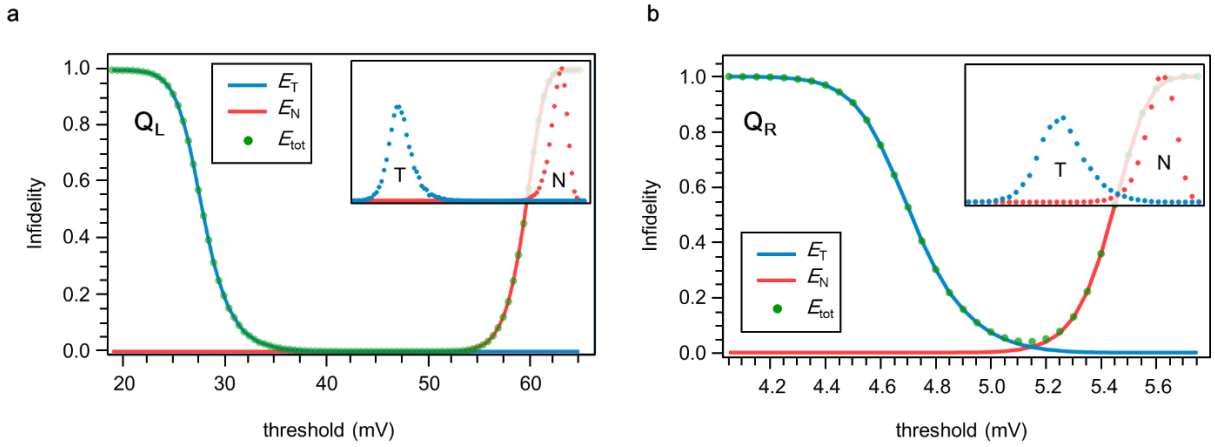

Supplementary Figure 6. Error simulation for direct peak detection scheme. a. (**b.**) The tunneling detection infidelity calculated from the rf-histogram in the inset. The histograms are constructed by sampling the peak values for Q_L (Q_R) single-shot traces without the spin relaxation, and thermal tunneling events to evaluate the tunneling detection infidelities without the CDS. For Q_L, the tunneling detection infidelities are below 0.00001% while for Q_R infidelities of $E_T \sim 2$ % , and $E_N \sim 2$ % are obtained at the optimal threshold.

The measurement fidelity and visibility are calculated for the direct peak detection scheme to explicitly show that the use of FPGA rather than CDS technique may extend the measurement fidelity and visibility with the same experimental parameters. Following the A. Morello *et al.*[6], single-shot traces were first simulated with the experimental parameters, and instead of passing through additional numerical CDS filter, the peak value (the minimum value) from each rf single-shot trace is sampled from 15,000 traces to construct the histogram shown in the insets of Supplementary Fig. 6a. and 6b. Because the short peaks or the full signal contrast cannot be perfectly detected with the CDS due to its limited bandwidth, the tunneling detection fidelities are naturally higher for the FPGA case. With the same τ_{out}, T_1, α_1 , α_2, and β, the measurement fidelity of Q_L (Q_R) is estimated as 94 % (88.8 %). We claim that the fidelities can further be higher if the FPGA-based readout is applied because the large peak separation would allow faster single-shot measurements with faster tunneling rates which would result in less relaxation due to lower τ_{out}/T_1.

Supplementary Note 7. Leakage error analysis due to Landau-Zener transition

We estimate the Landau-Zener transition probability during the fast ramp time by solving the time-dependent Schrodinger equation with the typical ST_0 qubit Hamiltonian[7]. We put the measured parameters such as the tunnel coupling strength, pulse rise time, pulse amplitude, and the magnetic field differences into the numerical simulation, and obtained the time trace of (2,0)S along the evolution time up to 10 ns. As the decoherence of the system is not considered in the simulation, the resultant trace (Supplementary Fig. 7) exhibits non-decaying oscillatory behavior in the 0 ~ 3% range which averages to 1.7%. We therefore conclude that the leakage probability and its effect to the visibility is not significant.

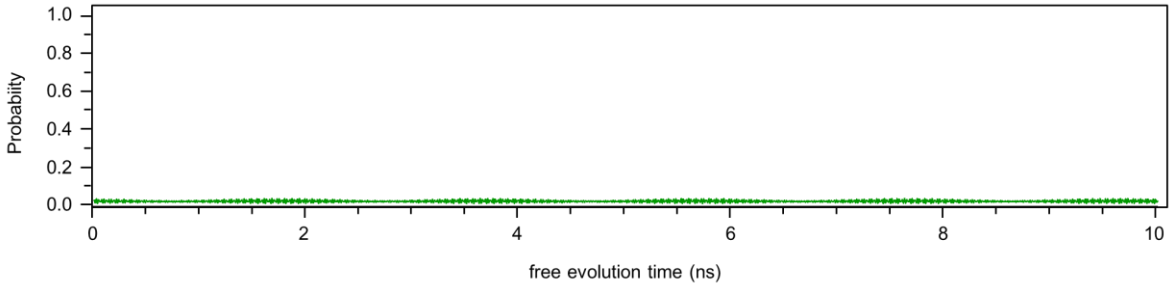

Supplementary Figure 7. The (2,0)S probability along the free evolution time. Time evolution of the (2,0)S state probability under the typical ST_0 qubit Hamiltonian is numerically obtained by putting the experimental parameters. The simulation yields 1.7% (2,0)S average occupation probability during the qubit manipulation time.

Supplementary Note 8. Measurement setup

A rf-single electron transistor (rf-set) sensor is operated to detect the charge states of the ST_0 qubits in our device. For the rf-reflectometry, impedance matching tank circuit as shown in Supplementary Fig. 8 is attached to the rf-ohmic contact of the device, and the 100 pF capacitor is connected in series to the other ohmic contact (depicted on the micromagnet) to serve as a rf-ground. With the inductor value L = 1500 nH and the parasitic capacitance C_p = 1.4 pF of the circuit board, the resonance frequency is about 110MHz, and the impedance matching occurs at rf-set sensor resistance approximately 0.5 h/e^2 where h is Plank's constant and e is the electron charge. A commercial high frequency lock-in amplifier (Zurich Instrument, UHFLI) is used as the carrier generator, rf demodulator for the homodyne detection, and further signal processing such as gated integration and timing marker generation. Carrier power of -40dBm power is generated at room temperature and attenuated through the attenuators and the directional coupler by -50 dB in the input line. The reflected signal is first amplified by 25 dB with commercial cryogenic amplifier (Caltech Microwave Research Group, CITLF2), and further amplified by 50 dB at room temperature using a home-made low-noise rf amplifier. Demodulated signal is acquired with a data acquisition card (National Instruments, NI USB-9215A) for raster scanning and also boxcar-averaged with the gated integrator module in the UHFLI for the correlated double sampling described above. For single-shot readout, the CDS output is counted with a high-speed commercial photon counter (Stanford Research Systems, SR400 dual gated photon counter). A commercial multichannel scalar (Stanford Research Systems, SR430 multichannel scaler & average) is also used for time correlated pulse counting for tunneling rate calibration.

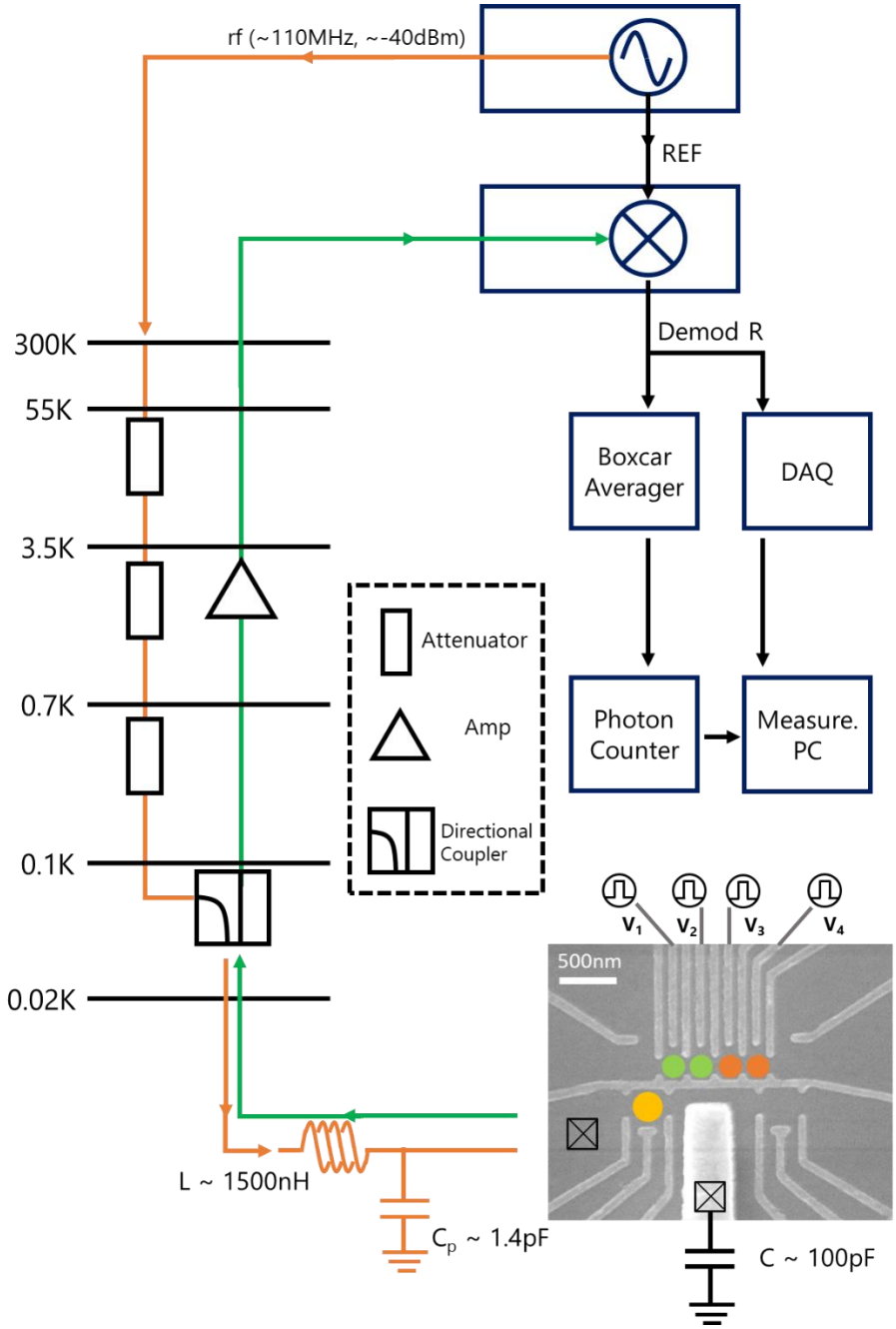

Supplementary Figure 8. The measurement setup for radio frequency (rf)-reflectometry, and the signal block diagram. Impedance matching tank-circuit (L~1500 nH, C_p ~ 1.4pF) is attached to the rf-set sensor Ohmic contact for homodyne detection. Orange (green) line indicates the input (reflected) signal. Reflected signal is demodulated and processed for single-shot event counting as shown in the block diagram.

Supplementary References

1. Elleaume, P., Chubar, O. & Chavanne, J. Computing 3D magnetic fields from insertion devices. in *Proceedings of the 1997 Particle Accelerator Conference (Cat. No.97CH36167)* vol. 3 3509–3511 vol.3 (1997).
2. Chubar, O., Elleaume, P. & Chavanne, J. A three-dimensional magnetostatics computer code for insertion devices. *J. Synchrotron Rad.* **5**, 481–484 (1998).
3. Pla, J. J. *et al.* A single-atom electron spin qubit in silicon. *Nature* **489**, 541–545 (2012).
4. Barthel, C., Reilly, D. J., Marcus, C. M., Hanson, M. P. & Gossard, A. C. Rapid single-shot measurement of a singlet-triplet qubit. *Phys. Rev. Lett.* **103**, 160503 (2009).
5. Nakajima, T. *et al.* Robust single-shot spin measurement with 99.5% fidelity in a quantum dot array. *Phys. Rev. Lett.* **119**, 017701 (2017).
6. Morello, A. *et al.* Single-shot readout of an electron spin in silicon. *Nature* **467**, 687–691 (2010).
7. Stepanenko, D., Rudner, M., Halperin, B. I. & Loss, D. Singlet-triplet splitting in double quantum dots due to spin-orbit and hyperfine interactions. *Phys. Rev. B* **85**, 075416 (2012).